THE JOURNAL OF CHEMICAL PHYSICS **139**, 124318 (2013)

The vibrational dependence of dissociative recombination: Cross sections for N_2^+

Steven L. Guberman[a)]
Institute for Scientific Research, 22 Bonad Road, Winchester, Massachusetts 01890, USA

(Received 30 June 2013; accepted 3 September 2013; published online 30 September 2013)

Theoretical *ab initio* calculations are reported of the cross sections for dissociative recombination of the lowest four excited vibrational levels of N_2^+ at electron energies from 0.001 to 1.0 eV. Rydberg vibrational levels contributing to the cross section structures are identified as are dissociative channels contributing more than 10^{-16} cm^2 to the total cross sections. In contrast to the prior study of v = 0 (S. L. Guberman, J. Chem. Phys. **137**, 074309 (2012)), which showed $2\,^3\Pi_u$ to be the dominant dissociative channel, $4^3\Pi_u$ is dominant for v = 1. Both 2 and $4^3\Pi_u$ are major routes for dissociative recombination from v = 2–4. Other routes including $2^3\Sigma_u^+$, $3^3\Pi_u$, $2^1\Pi_u$, $2^3\Pi_g$, $2^1\Sigma_g^+$, $1^1\Delta_g$, and $b'^1\Sigma_u^+$ are significant in narrow energy ranges. The results show that minor dissociative routes, included here for N_2^+, must be included in theoretical studies of other molecular ions (including the simplest ions H_2^+ and H_3^+) if cross section agreement is to be found with future high resolution dissociative recombination experiments. The calculated predissociation lifetimes of the Rydberg resonances are used in a detailed comparison to two prior storage ring experiments in order to determine if the prior assumption of isotropic atomic angular distributions at "zero" electron energy is justified. The prior experimental assumption of comparable cross sections for v = 0–3 is shown to be the case at "zero" but not at nonzero electron energies. Circumstances are identified in which indirect recombination may be visualized as a firefly effect. © *2013 AIP Publishing LLC*. [http://dx.doi.org/10.1063/1.4821595]

I. INTRODUCTION

The dissociative recombination (DR) of N_2^+ is described by

$$N_2^+(v) + e^- \rightarrow N + N, \tag{1}$$

where e^- is an electron, v denotes the vibrational level, and the product N atoms can be electronically excited. Because of the absence of a dipole moment, excited vibrational levels in the ground electronic state of N_2^+ have very long radiative lifetimes. Indeed, they may last longer than the duration of most experiments if they are not relaxed by collision or destroyed by reaction. This can present an experimental challenge if the ions are generated with a substantial degree of vibrational excitation and the aim is to determine rate constants for individual levels. DR cross sections, $\sigma(v)$, and rate constants, $\alpha(v)$, are known to be sensitive to v.[1] This sensitivity and the unknown vibrational states of the recombining ions has been the source of disagreement in deduced rate constants among experiments and between experiments and theory over the course of many years.[1] Clearly, if one does not know the experimental vibrational population and the level specific cross sections, a laboratory cross section or rate constant has limited application. For Earth, ionosphere models have derived the vibrational distributions and have shown that near 450 km, 45% (Ref. 2) and 50% (Ref. 3) of the ground electronic state of N_2^+ is vibrationally excited. 300 km above the surface of Mars, 50% of the N_2^+ is vibrationally excited.[4] Vibrational excitation at these altitudes arises from photon emission from electronically excited N_2^+ in allowed transitions to the ion ground state.[4] The v = 0 level of the first excited electronic state, $A^2\Pi_u$, lies between the v = 4 and v = 5 levels of the $^2\Sigma_g^+$ ground state allowing the lowest five vibrational levels of the ground ion to be very long lived. DR cross sections from the lowest four excited vibrational levels are the subjects of this paper.

In a previous paper,[5] theoretical calculations of the cross section and rate constant for the ground vibrational level are reported. Fourteen electronic dissociative states, identified as important for describing DR from the lowest 5 ion vibrational levels are included. The importance of a dissociative state is dependent upon the position relative to the 5 ion vibrational levels and the magnitude of the electron capture width. Diabatic dissociative states are described with Gaussian basis sets that exclude Rydberg character. Orbitals are determined in Complete Active Space Self Consistent Field (CASSCF) calculations.[6] Configuration interaction (CI) calculations used the CASSCF wave function as reference with the 2σ orbitals active. CI calculations are done by the direct CI approach[7] of the Molecule-Sweden programs[8] and by the internally contracted Multireference CI (MRCI)[9] approach of the MOLPRO programs.[10] Both the Molecule-Sweden and MOLPRO programs are used for the CASSCF calculations. The 14 dissociative routes are C-$4^3\Pi_u$, b, 2, $3^1\Pi_u$, $2^1\Sigma_g^+$, $b'^1\Sigma_u^+$, $2^3\Sigma_u^+$, $2^3\Pi_g$, $^3\Sigma_g^+$, $1^1\Delta_g$, and $2^3\Delta_g$. The first ten of these are shown in Fig. 1. Also included in the calculations is the

---

[a)] slg@sci.org

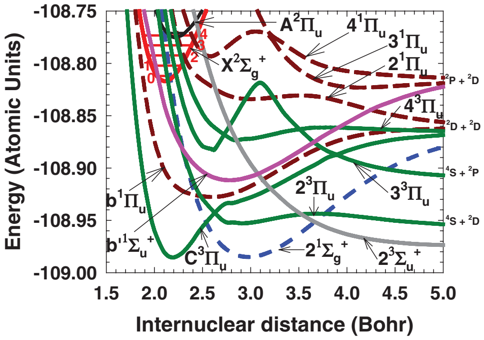

FIG. 1. Potential curves for DR of the $X^2\Sigma_g^+$ (red) state of N_2^+. The $A\,^2\Pi_u$ state (black) is in the upper left. The $^3\Pi_u$ (green), $^1\Pi_u$ (brown, dashed), $b'^1\Sigma_u^+$, (pink), $2^1\Sigma_g^+$ (blue, dashed-dotted), and $2^3\Sigma_u^+$ (gray) dissociative routes are shown with the states of the separated atoms.

excited $A\,^2\Pi_u$ ion as are the Rydberg states having the A state as core. Electron capture widths and quantum defects are calculated with CI wave functions that incorporate Rydberg orbitals determined in the Improved Virtual Orbital approach.[11] Cross sections and rate constants are determined with Multichannel Quantum Defect Theory (MQDT). The width and MQDT calculations are done with in house programs. The reader is referred to the previous paper[5] for additional details.

In Sec. II, the calculated cross sections at electron energies, ε, below 1 eV for the v = 1–4 levels are described. Section III has a comparison to prior research including spectroscopic and storage ring experiments and theory. The conclusions are in Sec. IV. Spherical Maxwellian rate coefficients, quantum yields, and a study of isotopomers will be reported separately.

II. CROSS SECTIONS

The shapes of cross sections in DR have been discussed previously.[5,12,13] Several processes which interfere with each other contribute to the shape. These include capture directly into the dissociative states, capture into ground and excited core Rydberg states, the emission of the captured electron (autoionization) prior to dissociation and dissociation along multiple routes to the atomic products. If Rydberg states are ignored, direct capture followed by dissociation (including the competing autoionization) leads to a mostly smooth cross section with abrupt decreases coming at ionization thresholds. In direct capture, if the Franck-Condon factor between the vibrational wave function for the ion and the neutral continuum dissociative states does not vary with ε, the cross section will vary as $1/\varepsilon$.[14] At energies above the lowest ion vibrational level, there is a dense forest of vibrationally excited Rydberg states having the ion ground state as the core. In N_2^+, there is also a forest of ground and excited Rydberg vibrational levels having the $A\,^2\Pi_u$ state as the core. Indirect DR occurs by capture into a Rydberg state followed by predissociation by the dissociative states. The interference between direct and indirect DR causes considerable structure in the cross section which can be described by a Fano like formula in the case of a single dissociative state and a single Rydberg level.[13] All the processes described here and the interference between them are included in the MQDT approach used for calculation of the cross sections.

The calculated v = 0 cross section has been presented previously.[5,15] Approximate positions of the $^3\Pi_u$ $X^2\Sigma_g^+$ core Rydberg resonances having v > 1 ion limits and $A^2\Pi_u$ core resonances with v ≥ 0 ion limits are given in Table I and shown (relative to the v = 0 ground state ion) in Figures 2 and 3, respectively. Resonances are denoted by (n, v) where n and v are the principal quantum number and Rydberg vibrational level, respectively. An A superscript denotes a level having the A core. High n Rydberg v = 0 levels having the X core do not play a role in DR since they lie below v = 0 of the ground state ion and the predissociation widths are very small. However, other levels with centers lying below the v = 0 ground ion can play a role in DR since they may have predissociation widths that allow some of the resonance to be above v = 0. Some levels below v = 0 are given in Figures 2 and 3. The positions are determined from the R dependent quantum defects described previously.[5] Resonance positions in Table I are approximate because they do not account for the widths and shifts that are due to interaction with the dissociation and ionization continua.

“Complex resonances” in which low n, high v interlopers interfere with higher n, lower v Rydberg levels in an autoionization continuum were discussed by Raoult and Jungen[16] in the photoionization of H_2. Interaction between the components of a complex resonance allows the higher n, lower v resonances to borrow oscillator strength from the low n resonances leading to anomalous spectra with intensities that do not fall off as n^{-3}. Complex resonances in photoionization lying between the v = 0 and v = 1 levels of $X^2\Sigma_g^+$, N_2^+ have been identified experimentally[17] and theoretically.[18] In photoionization, these resonances have allowed transitions from $X^1\Sigma_g^+$ and necessarily involve upper levels of $^1\Pi_u$ and $^1\Sigma_u^+$ symmetry. The previous work[17,18] has identified a complex resonance lying just below $X^2\Sigma_g^+$, v = 1 composed of a $(4, 0)^A$ σ_g $^1\Pi_u$ level and high n levels (>15, 1) of the $np\pi_u\,^1\Pi_u$ series with $X^2\Sigma_g^+$, v = 1 as the series limit. Complex resonances also occur in the DR of N_2^+, but although the $^1\Pi_u$ and $^1\Sigma_u^+$ valence and Rydberg states play important roles at isolated energies, the major electronic symmetry for DR is $^3\Pi_u$. To our knowledge, N_2 complex resonances in $^3\Pi_u$ symmetry have not been previously identified. Figures 2 and 3 and Table I show many possibilities for these complex resonances below each of the X and A state vibrational thresholds, some with multiple interlopers. By analogy to the $^1\Pi_u$ complex resonance, $(4, 0)^A$ $^3\Pi_u$ lies just below $X^2\Sigma_g^+$, v = 1 where it will interact with the (high n, 1) $^3\Pi_u$ levels and the continuum due to $X^2\Sigma_g^+$, v = 0.

In the discussion below, the analysis uses the resonance predissociation widths and lifetimes calculated from the matrix elements that enter the MQDT calculations. The predissociation width is given by

$$\Gamma^d_{n^*,v} = 2\pi\,|\langle\Psi^d\chi^d\,|H|\,\Psi_{n*}\chi_v\rangle|^2, \tag{2}$$

where Ψ^d and χ^d are electronic and continuum nuclear wave functions for the dissociative state and H is the electronic Hamiltonian. n^* and v denote the effective principal quantum

TABLE I. Energies (eV) of the np π_u, ${}^3\Pi_u$ Rydberg states of the X and A core states of N_2^+ for n ≤ 10.

n	v	Core	Energy above v = 1	Energy above v = 2	Energy above v = 3	Energy above v = 4
5	0	A	− 0.0011			
4	6	X	0.0060			
8	2	X	0.0088			
4	3	A	0.018			
5	4	X	0.035			
6	3	X	0.036			
3	12	X	0.048			
9	2	X	0.068			
10	2	X	0.11			
3	13	A	0.18			
7	3	X	0.18			
5	1	A	0.23			
4	4	A	0.24	− 0.028		
4	7	X	0.25	− 0.015		
3	13	X	0.27	0.003		
8	3	X	0.27	0.003		
5	5	X	0.29	0.021		
6	4	X	0.29	0.026		
6	0	A	0.31	0.039		
9	3	X	0.33	0.062		
3	14	A	0.36	0.097		
10	3	X	0.37	0.10		
5	2	A	0.46	0.19		
7	0	A	0.47	0.21		
3	14	X	0.49	0.22		
4	8	X	0.49	0.23	− 0.035	
8	4	X	0.53	0.26	− 0.0014	
5	6	X	0.54	0.27	0.0084	
6	1	A	0.54	0.27	0.010	
6	5	X	0.55	0.28	0.018	
3	15	A	0.55	0.28	0.019	
8	0	A	0.57	0.31	0.046	
9	4	X	0.59	0.32	0.057	
10	4	X	0.63	0.36	0.098	
9	0	A	0.64	0.37	0.11	
4	6	A	0.67	0.40	0.14	
5	3	A	0.68	0.42	0.15	
10	0	A	0.68	0.42	0.16	
7	5	X	0.69	0.42	0.16	
3	15	X	0.70	0.43	0.17	
7	1	A	0.71	0.44	0.18	
3	16	A	0.73	0.46	0.20	
4	9	X	0.73	0.46	0.20	
6	2	A	0.77	0.50	0.24	− 0.019
8	5	X	0.78	0.51	0.25	− 0.0055
5	7	X	0.78	0.52	0.25	− 0.0032
6	6	X	0.80	0.53	0.27	0.0094
8	1	A	0.81	0.54	0.28	0.020
9	5	X	0.84	0.57	0.31	0.053
9	1	A	0.87	0.60	0.34	0.086
10	5	X	0.88	0.61	0.35	0.094
4	7	A	0.88	0.61	0.35	0.10
3	17	A	0.90	0.64	0.37	0.12
5	4	A	0.90	0.64	0.38	0.12
3	16	X	0.91	0.64	0.38	0.12
10	1	A	0.92	0.65	0.39	0.13
7	2	A	0.93	0.67	0.40	0.15
7	6	X	0.94	0.67	0.41	0.15
4	10	X	0.97	0.70	0.44	0.18
6	3	A	0.99	0.72	0.46	0.21
5	8	X	1.0	0.76	0.50	0.24
8	6	X	1.0	0.76	0.50	0.24
8	2	A	1.0	0.77	0.51	0.25
6	7	X	1.0	0.77	0.51	0.25
3	18	A	1.1	0.81	0.55	0.29
4	8	A	1.1	0.82	0.56	0.30
9	6	X	1.1	0.82	0.56	0.30
9	2	A	1.1	0.83	0.57	0.31
3	17	X	1.1	0.85	0.58	0.33
5	5	A	1.1	0.85	0.59	0.34
10	6	X	1.1	0.86	0.60	0.34
10	2	A	1.1	0.88	0.62	0.36
7	3	A	1.2	0.89	0.63	0.37
7	7	X	1.2	0.92	0.66	0.40
4	11	X	1.2	0.93	0.67	0.41
6	4	A	1.2	0.94	0.68	0.43
3	19	A	1.2	0.98	0.72	0.46
8	3	A	1.3	0.99	0.73	0.47
5	9	X	1.3	0.99	0.73	0.47
8	7	X	1.3	1.0	0.75	0.49
6	8	X	1.3	1.0	0.75	0.50
4	9	A	1.3	1.0	0.76	0.50
3	18	X	1.3	1.0	0.78	0.53
9	3	A	1.3	1.1	0.79	0.54
9	7	X	1.3	1.1	0.80	0.55
5	6	A	1.3	1.1	0.81	0.55
10	3	A	1.4	1.1	0.84	0.58
10	7	X	1.4	1.1	0.84	0.59
7	4	A	1.4	1.1	0.85	0.59
3	20	A	1.4	1.1	0.88	0.62
4	12	X	1.4	1.2	0.89	0.63
7	8	X	1.4	1.2	0.90	0.64
6	5	A	1.4	1.2	0.90	0.64
8	4	A	1.5	1.2	0.95	0.69
4	10	A	1.5	1.2	0.96	0.70
5	10	X	1.5	1.2	0.97	0.71
3	19	X	1.5	1.2	0.98	0.72
8	8	X	1.5	1.2	0.99	0.73
6	9	X	1.5	1.3	0.99	0.73
9	4	A	1.5	1.3	1.0	0.76
5	7	A	1.5	1.3	1.0	0.76
3	21	A	1.6	1.3	1.0	0.79
9	8	X	1.6	1.3	1.0	0.79
10	4	A	1.6	1.3	1.1	0.80
7	5	A	1.6	1.3	1.1	0.81
10	8	X	1.6	1.3	1.1	0.83
4	13	X	1.6	1.4	1.1	0.85
6	6	A	1.6	1.4	1.1	0.86
7	9	X	1.7	1.4	1.1	0.88
4	11	A	1.7	1.4	1.2	0.90
15	4	A	1.7	1.4	1.2	0.90
14	8	X	1.7	1.4	1.2	0.91
8	5	A	1.7	1.4	1.2	0.91
3	20	X	1.7	1.4	1.2	0.91
5	11	X	1.7	1.5	1.2	0.94

TABLE I. (*Continued.*)

n	v	Core	Energy above v = 1	Energy above v = 2	Energy above v = 3	Energy above v = 4
3	22	A	1.7	1.5	1.2	0.95
5	8	A	1.8	1.5	1.2	0.96
6	10	X	1.8	1.5	1.2	0.97
8	9	X	1.8	1.5	1.2	0.97
9	5	A	1.8	1.5	1.2	0.98
10	5	A	1.8	1.5	1.3	1.0

number and bound vibrational level of the Rydberg state. The predissociation lifetime is obtained by inverting (2) and multiplying by $\hbar$.

Predissociation lifetimes are important because if predissociation is much faster than rotation, the angular distribution of the dissociating N atoms, determined by the electronic symmetry of the incoming electron,[19] must be taken into account in determining quantum yields in the storage ring experiment (see below). If the opposite is the case, the angular distributions may be isotropic, independent of electronic symmetry.

Using Eq. (2) for all n $\leq$ 20 $^3\Pi_u$ Rydberg levels within 1 eV electron energy above the ion levels undergoing DR, predissociation lifetimes range from 8.8×10^{-15} s to 3.9×10^{-9} s. Fast predissociation occurs mostly in low n states which energetically requires high v.

In the previously reported calculations on DR from the ground vibrational level,[5] 18 vibrational levels were used in the ground and A core states. However, in order to include all Rydberg levels above the v = 2–4 ground ion levels for electron energies up to 1 eV, 23 ion levels are included in both the X and A core states reported here.

A. v = 1

The calculated total v = 1 cross section is shown in Fig. 4 for $0.001 \leq \varepsilon \leq 0.1$ eV as are the channel contributions greater than 10^{-16} cm^2. The total $^3\Pi_u$ contribution (dashed black line) nearly overlaps the total cross section (red solid line) over much of this energy range except for isolated energies and near 0.03 eV where a broad peak arises due to $^1\Pi_u$ (see below). For energies below 0.1 eV, the $4^3\Pi_u$ state is dominant followed by $2^3\Pi_u$. (4, 6) $^3\Pi_u$ is the lowest energy resonance and appears with a dip at 0.0059 eV. Interference with the (8, 2) $^3\Pi_u$ level leads to a peak near 0.008 eV which appears in each of the four $^3\Pi_u$ contributions. The width (from Eq. (2)) of (4, 6) is 0.019 eV and it extends from below 0.0 eV up to 0.0078 eV. The predissociation lifetime of this resonance is 3.4×10^{-14} s so that DR at threshold will be much faster than rotation at 10^{-12} s (see below). The (8, 2) resonance has a width of 0.0026 eV and does not affect the threshold region. (The focus here on the threshold region is due to the comparison (given below) to storage ring measurements.) Note that the (8, 2) $^1\Pi_u$ resonance at 0.009 eV (due to dissociation along $b^1\Pi_u$) is apparent in the $^1\Pi_u$ contribution (and barely apparent in the total cross section). $(4, 3)^A$ $^3\Pi_u$ is the source of the peak at 0.014 eV with a width comparable to (8, 2) $^3\Pi_u$. An (8, 2) $^1\Sigma_u^+$ Rydberg state is the source of a small peak near 0.023 eV followed by a peak mostly due to dissociation along $2^1\Pi_u$ from $(6, 0)^A$ $^1\Pi_u$ with contributions from (5, 5) and (6,4) $^1\Pi_u$ at 0.030 eV. Near 0.036 eV, the (5, 4) and (6, 3) $^3\Pi_u$ (with dissociation along $4^3\Pi_u$) mix with $(3, 12)^A$ $^1\Pi_u$ (with dissociation along $2^1\Pi_u$) to form a peak.

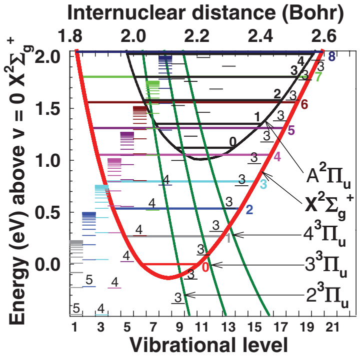

FIG. 2. The energies of $^3\Pi_u$ Rydberg levels with the ground core are shown with the N_2^+ X and A state and the 2, 3, and 4 $^3\Pi_u$ potential curves. The lowest member of each Rydberg series is labeled with the principal quantum number. The bottom abscissa denotes the Rydberg vibrational level. The top abscissa is only for the potential curves. The zero of energy is the v = 0 level of the ion ground state. Only Rydberg levels with n $\leq$ 20 are shown.

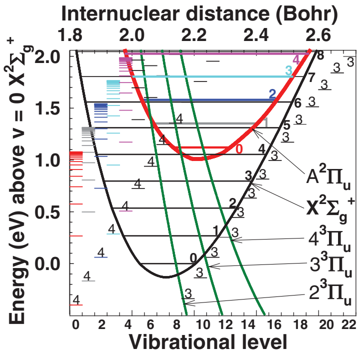

FIG. 3. Same as Figure 2 except the Rydberg levels are those having the A core.

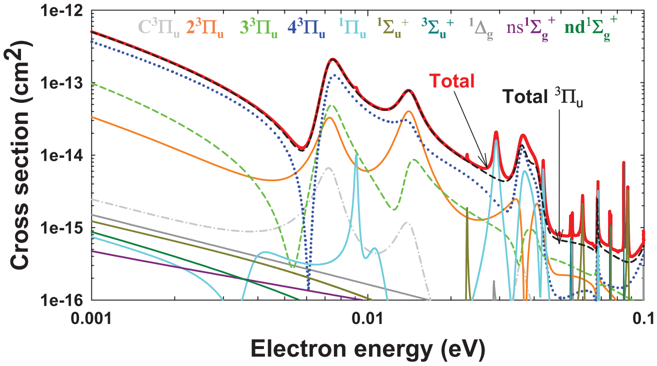

FIG. 4. The total cross section for v = 1 (red) and the total cross section of the four $^3\Pi_u$ states (black, dashed) is shown with the cross sections of other states. The color key identifying each state is given across the top of the figure.

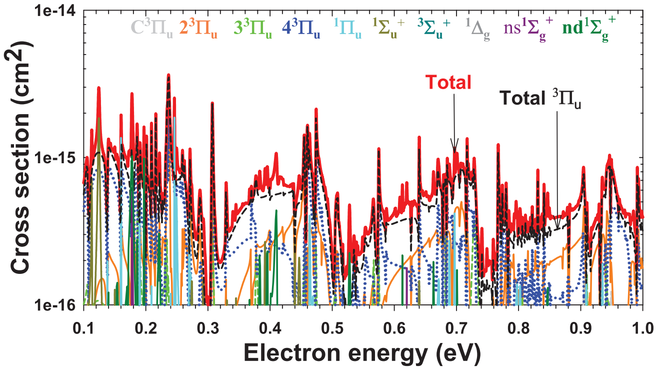

FIG. 5. Same as Figure 4 for v = 1 except that the electron energy range is 0.1–1.0 eV.

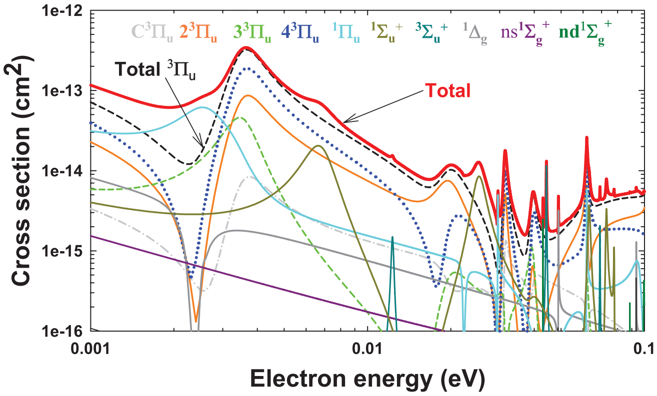

FIG. 6. Same as Figure 4 but for v = 2.

A sharp peak near 0.043 eV is due to both b and $2^1\Pi_u$ and the $(3, 12)^A$, (6, 3), and (5, 4) $^1\Pi_u$ states. Between 0.05 and 0.1 eV, six sharp peaks occur due to $^3\Sigma_u^+$, $^1\Sigma_u^+$, $^1\Pi_u$, and $^3\Pi_u$ Rydberg states.

Figure 5 shows that the cross section appears to be partitioned into 5 sections due to dips at 0.30, 0.52, 0.76, and 0.92 eV which follow the total $^3\Pi_u$ contribution to the cross section. The sources of these dips have been identified by repeating the cross section calculations with varying numbers of vibrational levels. The first three dips are due to (3, 13), (3, 14), and (3, 15) $^3\Pi_u$ states with unperturbed positions of 0.27 eV, 0.49 eV, and 0.70 eV (see Table I). The dip at 0.92 eV is due to $(3, 17)^A$ $^3\Pi_u$. Based upon the width calculations, (3, 13), (3, 14), (3, 15), and $(3, 17)^A$ extend from 0.27–0.33, 0.51–0.53, 0.73–0.79, and 0.88–0.96 eV. Each of these resonances has a lifetime less than 10^{-13} s.

In Figure 5, a series of narrow v = 2 resonances can be seen leading to the v = 2 ion threshold at 0.27 eV. A sharp peak at 0.31 eV is due to $^3\Pi_u$ $(6, 0)^A$. The sharp peak at 0.33 eV is due to $^3\Pi_u$ (9, 3). The cross section increases as the energy is increased (due to 2 and 4 $^3\Pi_u$) with structure due to $^3\Pi_u$ (10, 3) and $(3, 14)^A$ in addition to $^1\Sigma_g^+$ and $^1\Sigma_u^+$ Rydberg states. At higher energies, the high n, v = $3^3\Pi_u$ states interfere with $(7, 0)^A$ $^3\Pi_u$ near 0.47 eV. Above the v = 3 ion threshold at 0.53 eV (see Figure 5), the cross section rises following an envelope due to $2^3\Pi_u$ before abruptly falling at 0.73 eV due to the (3, 15) dip. Above the v = 5 ion threshold at 0.79 eV, the cross section rises again, reaching at peak at 0.94 eV due to $(3, 17)^A$ $^3\Pi_u$, the same state responsible for the dip at 0.02 eV lower energy. The v = 0, A core level is at 0.85 eV and the abrupt cutoff in structure due to $4^3\Pi_u$ and the $(n, 0)^A$ resonances is evident at this energy.

The largest resonance predissociation width (0.26 eV) from v = 1 DR is due to $(3, 19)^A$ at 1.25 eV above v = 1 with a lifetime of 2.5×10^{-15} s.

B. v = 2

These cross sections are shown in Figures 6 and 7. Interference between shifted (8, 3) and (3, 13) $^3\Pi_u$ resonances is the source of the first peak in the total cross section near 0.0035 eV. The latter resonance is the same one that caused a prominent dip in the v = 1 cross section at 0.30 eV above v = 1. (8, 3) has a width of 0.00068 eV and will not affect the threshold region. (3, 13) has a predissociation width of 0.026 eV and is present at threshold. This level predissociates rapidly with a lifetime of 2.6×10^{-14} s along $4^3\Pi_u$ and 2.7×10^{-14} s along $2^3\Pi_u$. The maximum in the $^1\Pi_u$ contribution near 0.0025 eV is due to (8, 3) predissociated by $2^1\Pi_u$. This level has a width of only 0.0002 eV. The 2, $4^3\Pi_u$ states dominate the cross section at higher energies. A bump in the cross section at 0.020 eV is due to (5, 5) $^3\Pi_u$. Peaks at 0.031 and 0.039 eV are due to $^3\Pi_u$ (6,4) and $(6, 0)^A$, respectively. From here until the peak near 0.062 eV due to (9, 3) $^3\Pi_u$ and (9, 3) $^1\Pi_u$, some of the structure is caused by minor DR routes: $^1\Sigma_u^+$, $2^3\Sigma_u^+$, and $1^1\Delta_g$. At higher energies, the cross section increases slightly before abruptly falling near 0.25 eV (see Figure 7) due to (3, 14) $^3\Pi_u$, the source of the dip at 0.52 eV in the v = 1 cross section. This dip is just below the v = 3 ion threshold at 0.26 eV. Below the dip, the structure is mostly due to the high n, v = 3 $^3\Pi_u$ resonances. The v = 1 dip at 0.76 eV appears at 0.49 eV. The dip near 0.62 eV is due to $(3, 17)^A$. There is a dip at 0.845 eV followed by a peak at 0.855 eV due to $^3\Pi_u$ $(5, 5)^A$. There are two prominent peaks at 0.89 and 0.94 eV due to $^3\Pi_u$ $(7, 3)^A$ and $(6, 4)^A$, respectively. Because of the many overlapping resonances, drops in the cross section (due to increased autoionization) just above the vibrational thresholds for the ground core v = 3 (0.26 eV), 4 (0.52 eV), 5 (0.77 eV) and the excited core v = 0 (0.59 eV) and v = 1 (0.82 eV) are not apparent.

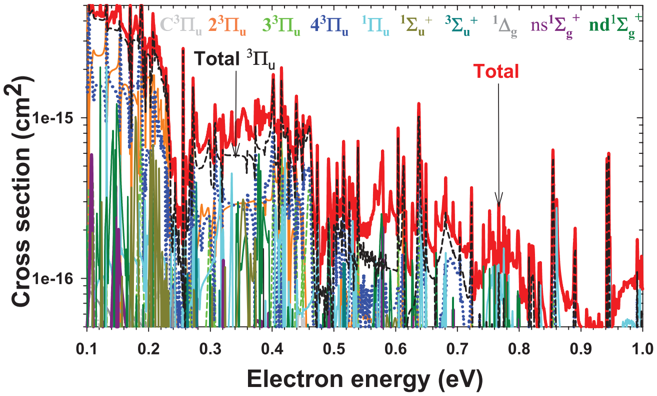

FIG. 7. Same as Figure 4 but for v = 2 and the electron energy range is 0.1–1.0 eV.

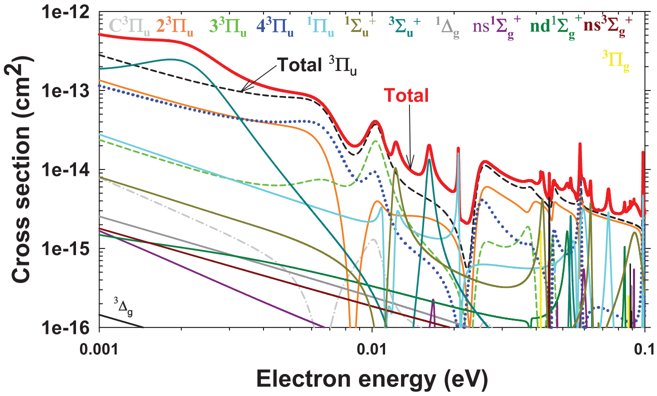

FIG. 8. Same as Figure 4 but for v = 3.

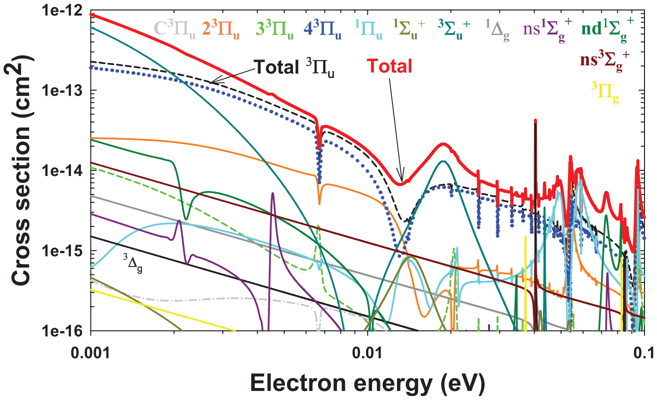

FIG. 10. Same as Figure 4 but for v = 4.

C. v = 3

At 0.002 eV, a cross section bump occurs (see Figure 8) due to (8, 4) $^3\Sigma_u^+$. This state has a predissociation lifetime of 1.4×10^{-13} s. In the threshold region, there are no $^3\Pi_u$ resonances contributing to the cross section with significant widths. Direct recombination is important in this region. At 0.0085 eV a sharp dip occurs in the $2^3\Pi_u$ cross section due to (5, 6). Similar but less sharp dips occur in the other $^3\Pi_u$ contributions (including $C^3\Pi_u$) at slightly displaced energies. At 0.010 eV, the $(6, 1)^A$ $^3\Pi_u$ causes a peak in all the contributing $^3\Pi_u$ dissociative states and a peak in the total cross section. The major contributor to this peak is a minor route, $3^3\Pi_u$, having an electron capture width of only 0.003 eV.[5] Peaks at 0.016 and 0.020 eV are due to (8, 4) $^3\Sigma_u^+$ and (6, 5) $^1\Pi_u$. The dip at 0.022 eV is due to (6, 5) $^3\Pi_u$. Continuing to 0.1 eV, the sharp structure is due to 2 and $4^3\Pi_u$, $2^1\Pi_u$, $^1\Sigma_u^+$, and both of the $^1\Sigma_g^+$ states having s and d wave capture.

Between 0.1 and 0.26 eV, Figure 9 shows a rich resonance structure with comparatively sparse structure above 0.26 eV. The first ion threshold is the ground core v = 4 level at 0.26 eV followed by the v = 0 excited core limit at 0.32 eV. Above 0.26 eV there are no v = 4 ground core levels and the resonance density decreases markedly. An analogous situation occurs above 0.32 eV. Below 0.32 eV, the high n, v = 0 excited core $^3\Pi_u$ resonances are too narrow to appear in the plot. Between 0.28 and 0.38 eV, $2^3\Pi_u$ dominates the cross section. The jagged total cross section just below the ground core v = 5 level at 0.51 eV is due to $^3\Pi_u$ Rydbergs. Structure due to terminating Rydberg series can be seen in the $^1\Pi_u$ and $^3\Pi_u$ contributions just below the v = 1 A core limit at 0.56 eV. Dense Rydberg structure is seen just below the 0.76 eV, v = 6, ground core limit followed by relatively sparse structure above this energy. At higher energies, increasing Rydberg structure leading to the v = 7 ground core (1.003 eV) and v = 3, A core (1.008 eV) limits can be seen.

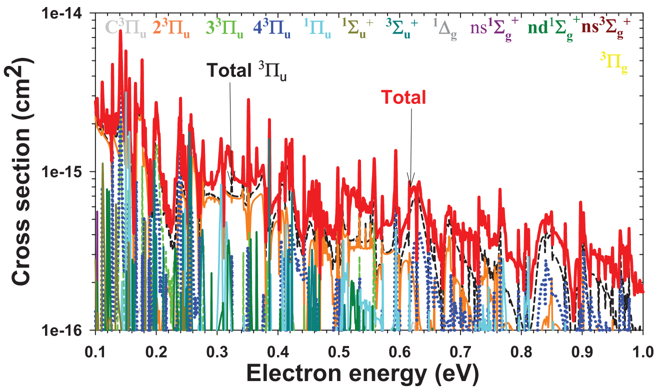

FIG. 9. Same as Figure 4 but for v = 3 and the electron energy range is 0.1–1.0 eV.

D. v = 4

At 0.001–0.002 eV, DR along $2^3\Sigma_u^+$ dominates. The nearly 4 orders of magnitude drop in the cross section between 0.001 and 0.01 eV is due to (8, 5) $^3\Sigma_u^+$ which has a predissociation lifetime of 1.5×10^{-13} s. Between 0.002–0.1 eV, the cross section is dominated by $4^3\Pi_u$ (see Figure 10). The small dip at 0.0067 eV is due to $(16, 0)^A$ $^3\Pi_u$. Higher members of this v = 0, A core series can be seen in the cross section up to the series limit at 0.067 eV. A peak near 0.019 eV is due to $^3\Sigma_u^+$ and the sharp spike at 0.040 eV is due to (8, 5) $^1\Delta_g$ and (9, 5) $^3\Delta_g$. The peak at 0.054 eV is due to (9, 5) $^3\Pi_u$. Figure 10 shows that (9, 3) $^1\Pi_u$ is the source of the dip at 0.053 eV and the two surrounding peaks. The peak at 0.094 eV is due to (10, 5) $^3\Pi_u$.

Between 0.1 and 0.5 eV, there are two series limits (see Figure 11). The v = 5 series with the ground core and the v = 1 series with the A core terminate at 0.25 and 0.30 eV, respectively. Near 0.28 eV, two high n Rydberg level peaks with the v = 1 A core are seen in the $4^3\Pi_u$ and $2^1\Pi_u$ channels. There are dense series of $^1\Sigma_u^+$ and $^3\Sigma_u^+$ Rydbergs just below the v = 5 ground core limit and below the v = 6 ground core limit at 0.50 eV. At 0.26–0.29 eV, the dominant dissociative states are 2 and $4^3\Pi_u$ and $2^1\Pi_u$. Sharp peaks at 0.30 and 0.31 eV are due to $(4, 8)^A$ and $(9, 2)^A$ $^3\Pi_u$ with the latter having a significant $^1\Pi_u$ component.

There are 6 ion limits at 0.5–1.0 eV above v = 4: v = 6, 7, and 8 ground core ion limits at 0.50, 0.75, and 0.99 eV and v = 2, 3, and 4 excited core limits at 0.53, 0.75, and 0.97 eV. Note that these ground and excited core limits are nearly coincident. Between 0.5 and 1.0 eV, the cross section is mostly dominated by $2^3\Pi_u$ with important contributions from $^1\Pi_u$, $^3\Sigma_u^+$, and $^1\Sigma_u^+$. (6, 8) and $(4, 9)^A$ $^3\Pi_u$ produce a high peak

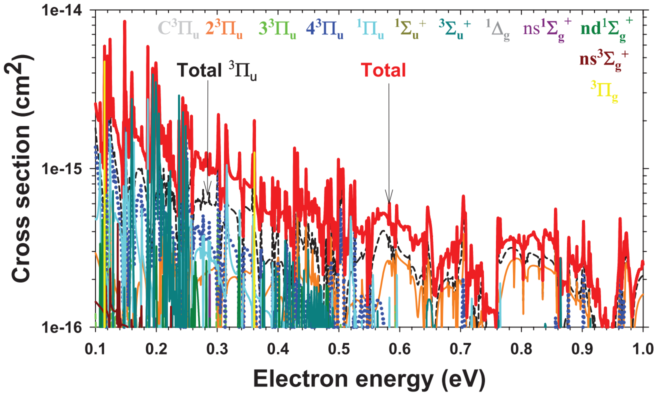

FIG. 11. Same as Figure 4 but for v = 4 and the electron energy range is 0.1–1.0 eV.

near 0.50 eV. A peak near 0.53 and a dip near 0.55 eV are due to $(9, 3)^A$ and $(5, 6)^A$ $^3\Pi_u$. At 0.94 eV a dip in the cross section occurs due to $(3, 22)^A$ $^3\Pi_u$. The width of the dip at the baseline cross section is 0.05 eV.

III. COMPARISON TO PRIOR RESEARCH

A. Theoretical and spectroscopic studies

Other than research reported from this laboratory, there has been only one prior study of N_2^+ DR.[20] A comparison to the current results has been reported previously.[5]

Positions of a few $^3\Pi_u$ Rydberg levels lying between v = 0 and v = 1 of $X^2\Sigma_g^+$ have been reported[21,23] The v = 1, n = 8, 9, and 10 Rydberg levels were found at 0.0125, 0.0632, and 0.1119 eV above v = 0.[21] Calculated values, using only the R dependent quantum defect, are given in Table VIII of Ref. 5: 0.0092, 0.068, and 0.11 eV. The previously[5] estimated uncertainty of 0.001 eV in the position of the n = 8 level was based solely upon the likely error in the calculated quantum defect. The theory does not include $f\pi_u$ character in the Rydberg orbital or the effect of rotationally dependent L-uncoupling between the $^3\Pi_u$ and $^3\Sigma_u^+$ Rydberg levels. These effects may account for the difference between theory and experiment. Experimental values[23] found for $(5, 0)^A$ and $(6, 0)^A$ are 0.20 and 0.54 eV above v = 0 compared to calculated positions of 0.27 and 0.57 eV (Table VIII of Ref. 5), respectively. A theoretical calculation found an excitation energy of 0.21 eV for $(5, 0)^A$.[22] In this calculation,[22] the positions of Rydberg levels were optimized in contrast to the MQDT approach in which a single quantum defect is used for the entire series. In the calculations reported here, only $ns\sigma_g$ was included in the description of the $^3\Pi_u$ Rydberg states with the $A^2\Pi_u$ core. $nd\sigma_g$ and $nd\delta_g$ were not included and this may contribute to the difference between theory and experiment.

Calculations reported here have neglected the spin-orbit splitting of the $A^2\Pi_u$ core, 0.009 eV.[23] The splitting of A core Rydberg levels should be addressed in future studies, especially in the low energy region. This splitting is similar to although smaller than the spin-orbit coupling in the ground state of O_2^+ where it leads to a coupling of $^1\Sigma_u^+$ and $^3\Sigma_u^-$ Rydberg states.[24]

B. Storage ring experiments

In merged beam[25] and storage ring experiments,[26,28] the discharge ion sources generate vibrationally hot ions in unknown vibrational distributions. For N_2^+, these ions do not relax in the course of the experiments. The ASTRID storage ring experiment[26] used $^{15}N^{14}N^+$ with the intent that the nonzero dipole would allow for vibrational relaxation. However, even these ions have vibrational lifetimes that are longer than the experimental measurement time. The ASTRID experiment was for “zero” eV electrons and no cross sections were reported. Quotes around zero indicate that the electron and ion beams are merged, aligned, and velocity matched so that the relative velocity along the ion or electron beam direction is zero. However, the electron beam has nonzero and unequal temperatures perpendicular and parallel to the beam such that the electron energy has a spread relative to the ion. (see Sec. III B 2 below).

1. Motional electric fields

In comparing storage ring derived cross sections to theoretically determined cross sections, important experimental characteristics must be recognized. First, motional electric fields induced by bending magnets can lead to field ionization of high Rydberg states. Rydberg states likely to be ionized have n ≥ 9 at ASTRID and CRYRING.[27] However, in N_2^+ DR, the products are (at low electron energies) all in valence states and field ionization does not affect the products. But can it affect the Rydberg states formed in indirect recombination? This too appears to be unlikely since, as described above, the maximum time for Rydberg state predissociation, 3.9×10^{-9} s, is much shorter than the time at CRYRING[28] or ASTRID[26] for neutral N_2 to pass from the cooler to the bending magnets. With the estimate that the first bending magnet is roughly the same distance from the electron cooler as the neutral detectors at CRYRING or ASTRID, the transit time from the center of the cooler to the magnet is about 1.0×10^{-6} s.

2. Electron velocity distribution

In the storage ring experiments, the electron beam does not have a spherical Maxwellian velocity distribution but because of the manner in which it is accelerated, it has a flattened velocity distribution in which the velocity perpendicular to the beam,$v_\perp$, has a wider spread than the velocity in the beam direction, $v_\parallel$. The spread is characterized by a perpendicular temperature, $T_\perp$, and a parallel temperature, $T_\parallel$. In the CRYRING[28] experiment, $kT_\perp = 0.01$ eV and $kT_\parallel = 0.0001$ eV.[29] At ASTRID,[26] the temperatures were 0.02 eV and 0.001 eV, respectively. In the following discussion, we take $kT_\parallel = 0.0$ eV. Taking v_i to be the velocity of an electron relative to an ion in the i-th direction, the total relative velocity is

$$v_{rel} = \left(v_x^2 + v_y^2 + v_d^2\right)^{\frac{1}{2}} = \left(v_\perp^2 + v_d^2\right)^{\frac{1}{2}} = \left(\frac{2}{m_e}\right)^{\frac{1}{2}} (E_\perp + E_d)^{\frac{1}{2}}, \tag{3}$$

where the electron beam is along the z axis and v_d is the detuning velocity, i.e., the velocity difference between the aligned electron and ion beam in the z direction. m_e is the electron mass.The measured rate constant can be calculated from

$$\alpha\left(E_{rel}, T_\perp\right) = \left(\frac{m_e}{kT_\perp}\right) \int_0^\infty e^{-\frac{m_e v_\perp}{2kT_\perp}} v_\perp \sigma\left(E_{rel}\right) v_{rel} dv_\perp . \tag{4}$$

Converting from a velocity to an energy integral gives

$$\alpha\left(E_d, T_\perp\right) = \left(\frac{2}{m_e}\right)^{\frac{1}{2}} \left(\frac{1}{kT_\perp}\right) \int_0^\infty e^{-\frac{E_\perp}{kT_\perp}} \times \sigma(E_\perp + E_d)(E_\perp + E_d)^{\frac{1}{2}} dE_\perp . \tag{5}$$

The flattened experimental rate constant, as a function of electron energy and $T_\perp$, is the directly measured quantity in a storage ring experiment. It is determined from measurements of the ion current, the ion velocity, the length of the region in which DR occurs and the number of neutral dissociation products detected per unit of time.[28] Inserting the theoretically calculated cross section into Eq. (5) provides a flattened rate constant for comparison to experiment. The experimentally derived cross section can be obtained from[28] $\sigma(E_d) = \alpha(E_d, T_\perp)/v_d$ above 0.1 eV and from a deconvolution procedure[28] for energies below 0.1 eV.

Flattened theoretical rate constants are shown in Fig. 12. The flattened rate constants bear little resemblance to rate constants (as a function of electron temperature) derived from a spherical average (to be published separately) of the theoretical cross sections. Indeed they retain considerable resonance structure. Of relevance to the discussion below is that at the lowest electron energies, the rate constants are similar for the lowest 5 vibrational levels. At 0.001 eV, the theoretical rate constants are in order of increasing vibrational quantum number: 2.4, 2.8, 2.5, 2.9, 2.5 × 10^{-7} cm^3/s) respectively. As the energy is increased, the rate constants diverge from one another up until 1 eV where there is some convergence. The greatest divergence is between v = 0 and v = 1 just below 0.1 eV.

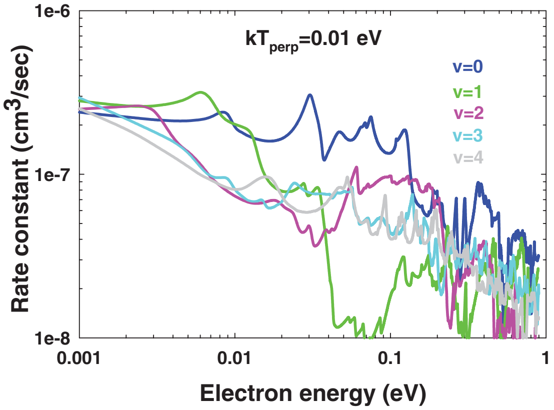

FIG. 12. Flattened theoretical rate constants for $T_\perp = 0.01$ eV.

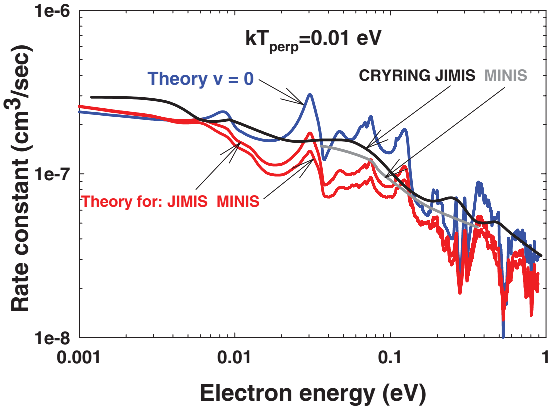

FIG. 13. Comparison of CRYRING and theoretical results. The CRYRING rate constants are shown with black and gray solid lines for the JIMIS and MINIS vibrational populations, respectively. The red lines denote the rate constants derived from the CRYRING vibrational populations using the theoretical flattened rate constants calculated for individual vibrational levels (see Figure 12).

3. Vibrational dependence of the flattened rate constant

Two sets of CRYRING rate constants are in Figure 13 for the ion sources JIMIS[30] and MINIS, shown with a black solid line and a gray solid line, respectively. The former source created cooler ions than the latter source but vibrational levels up to v = 3 were present in the ions from both sources. It is not clear why v = 4 was too small to be included since it cannot radiate to the A state. A measurement at $E_{rel} = 0$ of the product of the vibrational population (normalized to 1) multiplied by the vibrational level specific rate constant for JIMIS (v = 0: v = 1: v = 2: v = 3) is (0.46: 0.27: 0.10: 0.16) and for MINIS is (0.30: 0.31: 0.19: 0.18). Note that the components of the products, i.e., the populations and the rate constants, were unknown. The similarity of the magnitudes of the JIMIS and MINIS rate constants led the experimentalists to conclude that the rate constants were similar for all 4 vibrational levels: "We have concluded that the DR rates do not depend much on the vibrational state."[28] Figure 12 shows that this conclusion is confirmed by the theory presented here at the lowest energy, 0.001 eV, but not at higher energies. Therefore, a reasonable approximation is that at zero electron energy, the above relative products are approximately the relative vibrational populations. The red curves in Fig. 13 are total rate constants derived by multiplying the experimental populations at zero electron energy by the theoretical rate constants. JIMIS and MINIS red curves are still quite similar even though the rate constants for different vibrational levels are quite different at electron energies above 0.001 eV. If the theoretical rate constants at 0.001 eV are used, the derived populations are 0.50: 0.25: 0.10: 0.14 for JIMIS leading to a total JIMIS rate very similar to that shown in Figure 13.

The only apparent structures in the experimental rate constant shown in Figure 13 are a dip near 0.007 eV and slight bumps near 0.009, 0.05, and 0.2 eV. The bump at 0.009 eV appears to be the (8, 1) resonance which is centered at 0.009 eV above v = 0 in the theoretical cross section and is at 0.0125 eV in the spectroscopic results.[21] Although the experimental points are not dense, with the exception of the 0.05 eV bump, none of the other bumps appear in the flattened theoretical rate constants calculated at the experimental vibrational distributions. Peaks in the flattened theoretical total rate curves (red solid lines in Fig. 13) near 0.03, 0.05, 0.07, 0.12, 0.40, and 0.70 eV are due to DR from v = 0.[5] In agreement with experiment, the flattened theoretical MINIS curve is below the theoretical JIMIS curve. Comparing experimental and theoretical points, the theoretically flattened JIMIS and MINIS curves are on average 26% and 20% below the experimental rate constants, respectively. Uncertainties in the product of vibrational level rate constants and populations were not reported.[28]

Considering our early theoretical results,[31] it was observed[28] that "The $2^3\Pi_u$ repulsive state cannot dominate the DR process. Then the rate would change dramatically from vibrational level to vibrational level." Our early results showed that $2^3\Pi_u$ dominated the v = 0 rate constant but no theoretical conclusions were possible at that time about the role of other $^3\Pi_u$ states in the DR of excited vibrational levels. It has been shown here that indeed, both $2^3\Pi_u$ and $4^3\Pi_u$ play important roles in the DR of excited v. Nevertheless, it is also clear from Fig. 12 that the rate does "change dramatically from vibrational level to vibrational level" at nonzero electron energies. The cause of the similarity of the rate constants near zero electron energy is currently under study.

4. Product angular distributions

In the CRYRING experiment,[28] in order to derive quantum yields, a position and time sensitive detector was used. Quantum yields are determined from the separation between the 2 product N atoms recorded by the detector which has a screen mounted perpendicular to the neutral beam axis. The separation is dependent upon the distance from the cooler, the speed of the ions circulating in the ring, the ion beam radius, and the kinetic energy and angular distribution of the product atoms. ASTRID and CRYRING quantum yields were all determined at zero electron energy only for which it was assumed that the electron approaches the ion from all directions equally, i.e., isotropically. If this is the case, the neutral products also have an isotropic distribution; if not, the neutral products have an anisotropic distribution.[19] However, the isotropic assumption does not account for $kT_\perp = 0.01$ eV (or for $kT_\perp = 0.02$ eV at ASTRID). A more recent study[32] of the anisotropy of the product distributions in HD^+ indicates that there is a detectable anisotropy at zero detuning energy with $kT_\perp = 0.002$ eV, 5 and 10 times smaller than that for CRYRING and ASTRID, respectively. Therefore, anisotropy should be present in both the ASTRID and CRYRING experiments unless there was substantial rotational excitation in the recombining N_2^+. If the time to complete a rotation is less than the dissociation time, the anisotropy may not be present. For the CRYRING experiment, the rotational temperatures were reported to be 300 K for JIMIS and 600 K for MINIS for which the N_2^+ rotational population maxima come at J = 7 and J = 10, respectively.[33] These levels have rotational periods of 1.2 and 0.92 × 10^{-12} s respectively. At ASTRID, the product distributions were best fit with a rotational temperature of 1400 K. The maximum in the distribution comes at J = 15 for which the lifetime is 0.62 × 10^{-12} s. Results reported in Secs. II A–II D, show that the predissociation times in the threshold regions are all at least an order of magnitude shorter than these rotation times for v = 1 and v = 2 and a factor of 4 shorter for v = 3 and v = 4. For v = 0,[5] (8, 1) and $(4, 5)^3\Pi_u$ are in the threshold region. These resonances are at 0.0093 eV and 0.024 eV above v = 0 and have predissociation lifetimes of 1.5 × 10^{-12} and 1.6 × 10^{-13} s, respectively. The widths are 0.00043 eV and 0.0040 eV, respectively and neither resonance (except for the wings) is present at threshold. As noted above, the experimental[21] position of (8, 1) is 0.0033 eV higher than that reported here. The threshold region is dominated by direct recombination with an expected time for dissociation of about 3 × 10^{-15} s (from wavepacket calculations done in this laboratory). Therefore, at threshold, the slow rotation approximation is valid for each of the vibrational levels described here at 300 and 600 K but at 1400 K it is clearly valid for v = 0–2 but less so for v = 3 and v = 4. (v = 4 was not detected in either of the experiments.) The ASTRID and CRYRING experiments was not carried out at zero eV but at a detuning energy of zero eV with $kT_\perp = 0.02$ eV and 0.01 eV, respectively. This may be enough energy to reach slow predissociating resonances. Additional modeling of the flattened distribution is needed before definitive conclusions can be reached.

If dissociation is anisotropic in the CRYRING experiment, it is important to recognize that DR along v = 3 would not be properly described. At threshold (see Fig. 8), $^3\Sigma_u^+$ is dominant and the products will follow a $\cos^2\theta$ distribution. In the CRYRING experiment, in order to increase the signal, N atoms arriving at the detector from a single dissociation event were counted only if the difference in arrival times of the two atoms was less than 800 ps. This restricts the detection only to atoms that arise from dissociation in which the molecular axis is nearly perpendicular to the electron beam axis. This arrangement would miss the atoms arising from DR along $^3\Sigma_u^+$.

Another issue requiring further study is whether the vibrational population of the ion beam was changing with time. Separately, we will show that vibrational deexcitation coefficients are roughly of the same order of magnitude as the DR coefficients. This means that with time the vibrational population of the ions in the beams could tend toward v = 0.

5. Flattened total cross section

Figure 14 shows a comparison of the flattened theoretical cross sections with those from CRYRING. The theoretical cross section is for the JIMIS vibrational population and is approximated by simply dividing the flattened theoretical rate constant by the detuning velocity. The experimental cross section was derived by using a deconvolution procedure in the region below 0.1 eV.[28] Agreement between theory and experiment is quite good except that the theory shows structure which is absent in the experiment.

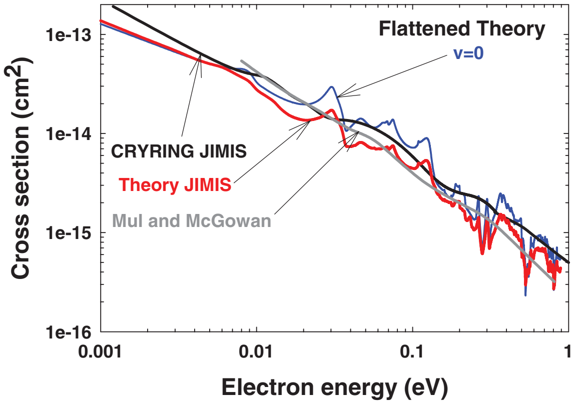

FIG. 14. The CRYRING cross section (black) and the theoretical cross sections (red) for the JIMIS population are shown with the theoretical cross section for v = 0 (blue) and the merged beam single pass cross section (gray).

C. Merged beam single pass experiments

Figure 14 also shows the results of a merged beam experiment[34] in which the electron and ion beams merge once instead of multiple times as in the storage ring experiments. The cross section data (as corrected and quoted in Ref. 25) show good agreement with the CRYRING and theoretical JIMIS population data. Of particular interest is that both merged beam and CRYRING cross sections have broad bumps centered near 0.06 and 0.3 eV and both are coincident between 0.01 and 0.03 eV. Is this agreement fortuitous or real? It is unlikely that both experiments had the same vibrational populations. The vibrational population of the merged beam experiment is unknown and some consideration was given to the possibility that the ion beam had electronically excited metastable states. They also reported a slope of $1/\varepsilon$ for the cross section in agreement with the theoretical and CRYRING results.

A later single pass merged beam[25] experiment found cross sections that were 3–10 times smaller than the earlier cross sections. An analysis[35] cast doubt on the validity of these results and also found that rate constants for v = 1 and v = 2 are smaller than those for v = 0. The effect of electron temperature upon the latter conclusion was not considered. Discussion of experimental and theoretical Maxwellian rate constants will be included in a follow-on paper.

D. Fireflies

In both the experiments discussed above and in flowing afterglows, indirect recombination is an ephemeral process in which Rydberg orbitals are formed and disappear within 8.8×10^{-15} s to 3.9×10^{-9} s. The expectation values of the "radii" of these orbitals scale as n^2.[36] For (8, 1) $^3\Pi_u$, the "radius" is approximately 95 a_o. In a storage ring experiment, the molecular ions circulate in the ring and pass through an electron cooler where recombination takes place. With 3.4 MeV kinetic energy, the time for the ions to transit the length of the electron cooler is about 10^{-7} s. These large Rydberg orbitals are formed and disappear before the ions have barely moved. If one tries to visualize the formation of these orbitals in a storage ring experiment, one would see these large orbitals popping up in random locations in the ion beam and disappearing. The evanescent nature of these large orbitals is reminiscent of fireflies on a warm summer evening.

For those levels having predissociation times on the order of 10^{-15} s, it is also possible that predissociation starts before capture is completed. In this case, is it possible that a complete Rydberg orbital does not form? Determination of the answer will require a time dependent description of the capture and dissociation.

IV. CONCLUSIONS

Theoretical cross section are calculated for the v = 1–4 vibrational levels of the N_2^+ ground state. 23 vibrational levels are included for the ion ground state and first excited state in addition to the Rydberg series leading to each of these levels. With 14 dissociative channels and two symmetries for the electron partial wave for $^1\Sigma_g^+$ and $^3\Sigma_g^+$, a total of $16 \times 23 \times 2 = 726$ Ry series are included and handled with the MQDT approach. Although $2^3\Pi_u$ and $4^3\Pi_u$ are the dominant dissociative routes, other routes included in the calculations make dominant cross section contributions in narrow energy intervals. The importance of an individual route is determined by its Franck-Condon factor, its electronic width and a complex interaction with other dissociative and resonance states. For v = 1, $3^3\Pi_u$ makes an important contribution even though its electron capture width[5] is only 0.002 eV near the ion R_e. For v = 1 and v = 2, the $2^1\Pi_u$ contribution is apparent in the total cross section as is that for $b'^1\Sigma_u^+$ for v = 2. For v = 3, $3^3\Pi_u$ is dominant near 0.01 eV and $b^1\Pi_u$, $^3\Sigma_u^+$, $2^1\Sigma_g^+$, and $^3\Pi_g$ contribute noticeably to the total cross section as does $^3\Sigma_u^+$, $^3\Pi_g$, $^3\Sigma_g^+$, $^1\Sigma_g^+$, $^3\Delta_g$, and $2^1\Pi_u$ for v = 4. The results indicate that accurate calculations of cross sections for other species such as H_2^+ and H_3^+ will also require the inclusion of minor dissociative routes.

Calculated predissociation lifetimes are so short that it is unlikely that the storage ring bending magnets can lead to field ionization. A comparison of predissociation lifetimes and rotational periods allows for an analysis of the need to account for product angular anisotropy in storage ring experiments. Experimental measurements of quantum yields are done near zero electron energy and it is shown that in this region, for both the ASTRID and CRYRING experiments, the slow rotation approximation is valid but less so for v = 3. The effect of $kT_\perp$ on the angular anisotropy is discussed but further research is needed in this area.

In contrast to the CRYRING conclusion that the rate constants for v = 0–4 are similar, the calculations show that this conclusion is valid at zero eV but not valid at higher energies where the v = 0 rate constant departs from those for v = 1–4. The total flattened rate constant calculated with the theoretical flattened rate constants for each vibrational level over the two CRYRING deduced vibrational distributions show much more structure than found in the experimental rate constant and are below the experimental results by averages of 26% and 20%.

For the flattened theoretical total cross section, there is good agreement with the CRYRING values and with those from a single pass merged beam experiment although neither experiment reproduces the structure seen by the theory.

The ephemeral nature of the Rydberg orbitals produced in indirect recombination is visualized as resembling a swarm of fireflies on a warm summer evening.

ACKNOWLEDGMENTS

I thank Professor J. B. A. Mitchell for information about the single pass merged beam experiments and Professor Mats Larsson, Professor Stefan Rosén, and Professor Wim van der Zande for supplying information about the CRYRING experiment. This research was supported by the National Science Foundation under Grant No. ATM-0838061 and by NASA under Grant No. NNX09AQ73G.

[1] A. I. Florescu-Mitchell and J. B. A. Mitchell, Phys. Rep. **430**, 277 (2006).
[2] M. R. Torr and D. G. Torr, Rev. Geophys. Space Phys. **20**, 91, doi:10.1029/RG020i001p00091 (1982).
[3] J. L. Fox and A. Dalgarno, J. Geophys. Res. **90**, 7557, doi:10.1029/JA090iA08p07557 (1985); J. L. Fox, *ibid.* **91**, 1731, doi:10.1029/JA091iA02p01731 (1986).
[4] J. L. Fox and A. Dalgarno, J. Geophys. Res. **88**, 9027, doi:10.1029/JA088iA11p09027 (1983); J. L. Fox, *ibid.* **98**, 3297, doi:10.1029/92JE02289 (1993); J. L. Fox and A. Hać, *ibid.* **102**(E4), 9191, doi:10.1029/97JE00086 (1997).
[5] S. L. Guberman, J. Chem. Phys. **137**, 074309 (2012).
[6] H.-J. Werner and P. J. Knowles, J. Chem. Phys. **82**, 5053 (1985).
[7] P. E. M. Siegbahn, A. Heilberg, B. Roos, and B. Levy, Phys. Scr. **21**, 323 (1980); P. E. M. Siegbahn, J. Chem. Phys. **72**, 1647 (1980).
[8] P. E. M. Siegbahn, C. W. Bauschlicher, B. Roos, P. R. Taylor, and J. Almlöf, Molecule-Sweden.
[9] H.-J. Werner and P. J. Knowles, J. Chem. Phys. **89**, 5803 (1988).
[10] H.-J. Werner and P. J. Knowles, R. D. Amos, A. Bernhardsson, A. Berning *et al.*, MOLPRO, version 2000.1, a package of *ab initio* programs, 2000, see http://www.molpro.net.
[11] W. J. Hunt and W. A. Goddard III, Chem. Phys. Lett. **3**, 414 (1969).
[12] A. Giusti, J. Phys. B **13**, 3867 (1980).
[13] S. L. Guberman, and A. Giusti-Suzor, J. Chem. Phys. **95**, 2602 (1991).
[14] J. N. Bardsley, J. Phys. B **1**, 349 (1968).
[15] In Table VIII of Ref. 5, the n = 4, v = 6 and the n = 4, v = 8 Rydberg levels at 0.27 and 0.76 eV, respectively, were omitted.
[16] C. Jungen and M. Raoult, Faraday Discuss. Chem. Soc. **71**, 253 (1981).
[17] P. M. Dehmer, P. J. Miller and W. M. Chupka, J. Chem. Phys. **80**, 1030 (1984).
[18] A. Giusti-Suzor and H. Lefebvre-Brion, Phys. Rev. A **30**, 3057 (1984).
[19] S. L. Guberman, J. Chem. Phys. **120**, 9509 (2004).
[20] H. H. Michels, "Theoretical determination of electronic transition probabilities for diatomic molecules," Technical Report No. AFWL-TR-72-1, 1972.
[21] S. W. Sharpe and P. M. Johnson, J. Chem. Phys. **85**, 4943 (1986).
[22] P. Cremaschi, A. Chattopadhyay, P. V. Madhavan and J. L. Whitten, Chem. Phys. **109**, 117 (1986).
[23] A. Lofthus and P. H. Krupenie, J. Phys. Chem. Ref. Data **6**, 113 (1977).
[24] S. L. Guberman, Science **278**, 1276 (1997).
[25] C. Noren, F. Yousif and J. B. A. Mitchell, J. Chem. Soc., Faraday Trans. 2 **85**, 1697 (1989).
[26] D. Kella, P. J. Johnson, H. B. Pedersen, L. Vejby-Christensen, and L. H. Andersen, Phys. Rev. Lett. **77**, 2432 (1996).
[27] A. Al-Khalili *et al.*, Phys. Rev. A **68**, 042702 (2003).
[28] J. R. Peterson, A. Le Padellec, H. Danared, G. H. Dunn, M. Larsson, A. Larson, R. Peverall, C. Strömholm, S. Rosén, M. af Ugglas, and W. J. van der Zande, J. Chem. Phys. **108**, 1978 (1998).
[29] S. Rosén and W. van der Zande, private communication (2013).
[30] This source was named in honor of Jim Peterson.
[31] S. L. Guberman, Geophys. Res. Lett. **18**, 1051, doi:10.1029/91GL01157 (1991); S. L. Guberman in *Dissociative Recombination: Theory, Experiment, and Applications*, edited by B. Rowe, J. B. A. Mitchell, and A. Canosa (Plenum, New York, 1993).
[32] S. Novotny *et al.*, "Anisotropic fragmentation in low energy dissociative recombination," J. Phys.: Conf. Ser. **192**, 012024 (2009).
[33] G. Herzberg, *Molecular Spectra and Molecular Structure, I. Spectra of Diatomic Molecules* (Van Nostrand Reinhold, New York, 1950), p. 124.
[34] P. M. Mul and J. W. McGowan, J. Phys. B **12**, 1591 (1979).
[35] D. R. Bates and J. B. A. Mitchell, Planet. Space Sci. **39**, 1297 (1991).
[36] T. F. Gallagher, *Rydberg Atoms* (Cambridge University Press, Cambridge, 1994).